SUPPORTING INFORMATION

Donor-Acceptor Molecular Architecture involving carbazole/pyrazine/anthraquinone units for Efficient Supercapacitor Applications

Sumit D. Ambore,[a,b] Chepuri R.K. Rao,[a,b,*] Sidhanath V. Bhosale,[a,b,*] Sheshanath V. Bhosale,[c,*]

[a]Polymers and Functional Materials Division, CSIR-Indian Institute of Chemical Technology, Hyderabad-500007, Telangana, India.

[b]Academy of Scientific and Innovative Research (AcSIR), Ghaziabad- 201002, Uttar Pradesh, India

[c]Department of Chemistry, School of Chemical Sciences, Central University of Karnataka, Kadaganchi, Kalaburagi-585 367, Karnataka, India

***Corresponding Authors:** ramchepuri@iict.res.in; bhosale@iict.res.in; bsheshanath@gmail.com; bsheshanath@cuk.ac.in

Experimental Section:

Materials

1,2-Diamino anthraquinone, and tris(dibenzylidine acetone) dipalladium (0) were procured from Sigma-Aldrich Pvt. Ltd., India and 4,4'dibromobenzil (>97%) and tri-tert-butyl phosphine tetrafluoroborate (>98%)were procured from TCI Chemicals Pvt. Ltd. Sodium *tert*-butoxide from Spectrochem Pvt. Ltd. Acetic acid, toluene and methanol were purchased from Finar Pvt. Ltd. Graphite foil (GF) purchased from Falcon Graphite Industries, India. Carbon black (super p-conductive), poly(vinylidene fluoride) $[-CH_2CF_2-]_n$ were procured from Alfa Aesar Hyderabad, India. TLC plates (Merck Co.) pre-coated with silica gel (40–60 mm, F254) were utilized and visualized using UV light (254 and 365 nm).

Structural Characterizations

^{1}H and ^{13}C NMR spectras were recorded on a Bruker Advanced 400 MHz and 500 MHz 100 and 125 MHz spectrometer at 300˚K, respectively. FT-IR spectras were recorded using Perkin Elmer Spectrum (Spectrum 100; PerkinElmer) instrument. MALDI-TOF measurements were performed by using Schimadzu Biotech Axima performance spectroscopic instrument. A field emission scanning electron microscope (FE-SEM) (Quanta FEG 250) was utilized for investigating the electrode morphology. Thermogravimetric analyses (TGA) was performed by using TGA-Q500 instrument under the N_2 atmosphere at heating rate of 10 ˚C min^{-1} up to 800 ˚C.

Electrochemical measurements

ZIVE LAB (MP 5) using electrochemical work station was used for recording electrochemical characterization of the solution as well as device. The electrochemical experiments were carried out at r.t. (~25˚C). Graphite foil electrode was utilized as working electrode, a platinum (Pt) wire and Ag/AgCl (sat KCl) as the counter and reference electrodes, respectively, for the three-electrode cell.1 M H_2SO_4aqueous solution was used as an electrolyte. The cyclic voltammetry (CV), galvanostatic charge-discharge (GCD), and electrochemical impedance spectroscopy (EIS) were utilized for the analysis of fabricated electrodes. At various scan rates from 5, 10, 20, 30, 50, 100, and 200 mV s^{-1}, three electrode CV experiments were performed. GCD was examined at various current densities of 0.5, 1, 2, 3, 4, 5, and 10 Ag^{-1}. EIS was examined at 0.01 Hz to 100 kHz frequency range at 0 V bias conditions with a 10 mV AC sinus perturbation.

Synthesis of 2,3-bis(4-bromophenyl)naphtho[2,3-f]quinoxaline-7,12-dione (AQ-Pyz-Br)

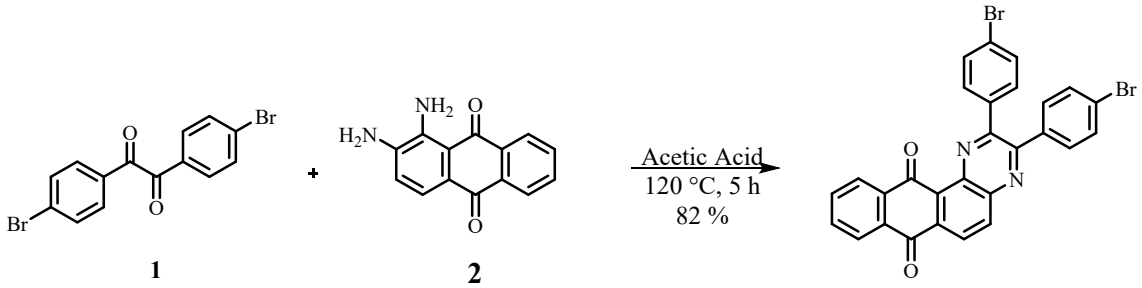

Scheme S1: Synthesis of AQ-Pyz-Br

A mixture of 1,2-bis(4-bromophenyl)ethane-1,2-dione (1) (0.920 g, 25 mmol) and 1,2-diaminoanthracene-9,10-dione (2)(0.595g, 25mmol) were dissolved in 20 mL of acetic acid and heated to reflux for 5h. The completion of reaction was confirmed by TLC. Then the reaction mixture was allowed to cool at r.t. and poured over crushed ice with constant stirring to obtain the orange colour solid. The obtained crude product was dried under vacuum and purified using column chromatography (eluent: n-hexane: $CHCl_3$; 60:40, *v/v* ratio) to yield a bright orange solid of ***AQ-Pyz-Br***(82 %). ^{1}H NMR (400 MHz, $CDCl_3$, δ ppm): 8.66 (1H, d, *J*=9.0 Hz), 8.45(1H, d, *J*=9.0), 8.29- 8.35 (2H, m), 7.78-7.88 (2H, m), 7.67-7.71(2H, m), 7.54-7.58 (6H, m); ^{13}C NMR (100 MHz, $CDCl_3$, δ ppm): 195.64 (C=O), 153.6, 153.07, 142.9, 140.2, 138.7, 137.2, 137.2, 137.0, 132.9, 132.3, 131.8, 131.4, 131.3, 130.3,130.1, 129.7, 128.6, 124.3, 124.1.

Synthesis of compound 3,6-di-tert-butyl-9H-carbazole (DTCz)

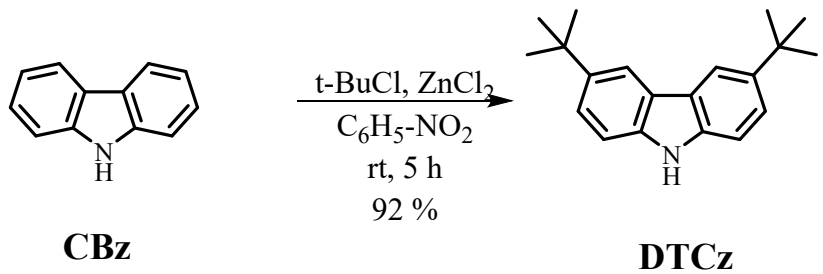

Scheme S2: Synthesis of DTCz.

Carbazole (CBz) (2.0g, 11.96mmol), was suspended in nitrobenzene 64mL under an argon atmosphere and anhydrous $ZnCl_2$(4.88g, 38.8mmol) was added. To this suspension was disappeared and colour turned from colourless to green grey. At r.t. the reaction mixture was stirred for 5 h and resulted into formation of colourless precipitate. By adding 65 mL of H_2O, the reaction was quenched. Then the mixture was extracted with CH_2Cl_2 (3×24 mL). The combined organic extracts were washed with H_2O (2 × 100 mL) and finally dried over $MgSO_4$. The solvent evaporation resulted into the white product in crude form. The crude product was purified by column chromatography (eluent: n-hexane: $CHCl_3$; 95:5, *v/v* ratio) of ***DTCz***(92%).^{1}H NMR (400MHz, $CDCl_3$): δ = 1.45 (s, 18H, $C(CH_3)_3$), 7.33(dd, *J* = 0.5, 8.5 Hz, 2H, ArH), 7.45 (dd, *J*= 2.0, 8.5 Hz, 2H, ArH), 7.85 (br, s, 1H, NH), 8.08 (d, *J*= 2.0 Hz, 2H, ArH); ^{13}C NMR (100MHz, $CDCl_3$, δ ppm): 142.2, 138.0, 123.5, 123.3, 116.2, 110.0, 34.73, 31.8.

Synthesis of 2,3-bis(4-(3,6-di-tert-butyl-9H-carbazol-9-yl)phenyl)naphtho[2,3-f] quinoxaline-7,12-dione (DTCz-Pyz-AQ)

AQ-Pyz-Br (1.00 g, 1.75 mmol) and the corresponding DTCz (1.17 g, 4.20 mmol) were dissolved in toluene, *t*-BuONa (0.50 g, 5.26 mmol) were subsequently added into the solution followed by pinch of tri-*tert*-butyl phosphine tetrafluoroborate and tris(dibenzylidene acetone) added. The resulting reaction mixture was heated to reflux for 12 h. After cooling to r.t. the reaction mixture was filtered through celite and the solvent was evaporated to dryness under vacuum. The crude product was purified by column chromatography on silica gel to afford ***DTCz-Pyz-AQ*** as dark red solid: 0.520 g (30 %); FT-IR (γ, cm^{-1} , KBr) 2957(C-H stretching), 2866 (C-H stretching), 1670 (C=O stretching), 1602 (C=C stretching), 807 (C=C bending); ^{1}H NMR (500 MHz, $CDCl_3$) δ 8.74 (d, *J* = 8.7 Hz, 1H, ArH), 8.57 (d, *J* = 8.7 Hz, 1H,ArH), 8.43 – 8.39 (m, 1H, ArH), 8.35 (dd, 1H, ArH), 8.16 (dd, 6H, ArH), 8.03 (d, 2H, ArH), 7.87 (m , 2H, ArH), 7.73 (d, *J* = 8.7 Hz, 4H, ArH), 7.50 (qd, 8H, ArH), (d, 36H,

CCH_3); ^{13}C NMR (100MHz, $CDCl_3$, δ ppm): 187.9, 180.6,145.8, 144.8, 142.5, 137.8, 137.4, 136.5, 136.1, 132.0, 131.7, 128.6, 128.1, 126.6, 126.0, 125.0, 124.5, 124.2, 117.6, 116.8, 116.5, 115.3, 113.1, 110.8, 109.6, 109.2, 34.8, 34.8, 31.7, 31.6; MALDI-TOF Calcd for $C_{68}H_{62}N_4O_2$ = 966.487 $[M]^+$; found 969.58 $[M+2H]^+$.

Cyclic voltammetry experiments for the energy band gap estimation:

The CV measurements were carried out by using the ZIVE LAB series potentiostat.0.1 M tetrabutylammonium hexafluorophosphate electrolyte was used for CV in DCM under N2 atmosphere.3 mm glassy carbon electrode, Ag/AgCl (sat KCl) and Pt wire as reference, working and counter electrode; (e) scan rate: 10 mV s^{-1}.

Electrode preparation:

The functioning electrode was imitated by creating a slurry from DTCz-Pyz-AQ. was used as the active component, super p-conductive carbon black served as the conductive agent, and polyvinylidene fluoride (PVDF) served as the binder. By grinding the three components in a 70:20:10 weight ratio, the components were thoroughly combined (14:4:2 mg). To create a uniform slurry, 6 mg of the finely powdered combination were then taken, dispersed in 0.6 mL of *N*-methyl-2-pyrrolidone (NMP) as a solvent, and sonicated for an hour. A drop of this slurry measuring 0.05 mL was cast onto a graphite foil (GF) measuring 1× 1 cm^2 area. The resulting slurry was suitably coated on graphite foil and allowed to dry for 12 h in a hot air oven at 80 °C. The electrode's active material mass was nearly ~1.5 mg. The electrode performance was investigated in a three- electrode supercapacitor device configuration. The fabricated electrode acts as the working electrode, whereas, platinum and Ag/AgCl (sat. KCl) act as the counter and reference electrodes, respectively. As an electrolyte aqueous 1 M H_2SO_4solution was used. All the experiments were conducted at r.t. (25 ˚C).

Two electrode symmetric fabrication:

The symmetric supercapacitor (SSC) device electrochemical system was performed by DTCz-Pyz-AQ/GF electrode materials and was examined . The two-electrode symmetric DTCz-Pyz-AQ/GF//DTCz-Pyz-AQ/GFsupercapacitordevice was assembled byutilizing Swagelok cell. A pair ofDTCz-Pyz-AQ/GF electrodes were employed as an anode and cathode electrode. A symmetric supercapacitor device was fabricatedusing two similar electrodes separated by cellulose. 1 M H_2SO_4 solution was used as an electrolyte.

Formulas used:

Specific capacitance from the three electrode CV studies.[S1]

$$C_{sp} = \frac{I \int dV}{2 \times v \times m \times \Delta V} \qquad 1$$

Specific capacitance from the three electrode GCD studies.[S2]

$$C_{sp} = \frac{I \times \Delta t}{m \times \Delta V} \qquad 2$$

Where C_{sp} represents the specific capacitance (Fg^{-1}), I represents the response current (mA), v represents the potential scan rate ($mV\ s^{-1}$), m represents the mass of the active material (g),Δt represents the discharge time (s), ΔV represents the voltage window (V).

Specific capacitance from the two electrode GCD studies.[S2]

$$C_{sp} = 4\left(\frac{I \times \Delta t}{m \times \Delta V}\right) \qquad 3$$

Where C_{sp} represents the specific capacitance (Fg^{-1}), I represents the response current (A), v represents the potential scan rate (mVs^{-1}), m represents the active material average mass of both electrodes (g), Δt represents the discharge time (s), ΔV represents the voltage window (V).

Energy density calculated from the two-electrode GCD analysis.[S2]

$$E = \frac{1}{8} \times C_{sp}(\Delta V)^2 \qquad 4$$

Power Density calculated from the two-electrode GCD analysis.[S2]

$$P = \frac{E}{\Delta t} \times 3600 \qquad 5$$

Where C_{sp} represents the specific capacitance (F g^{-1}), ΔV represents the voltage window (V), E represents the energy density (Wh kg^{-1}) and P represents the power density (W kg^{-1}).

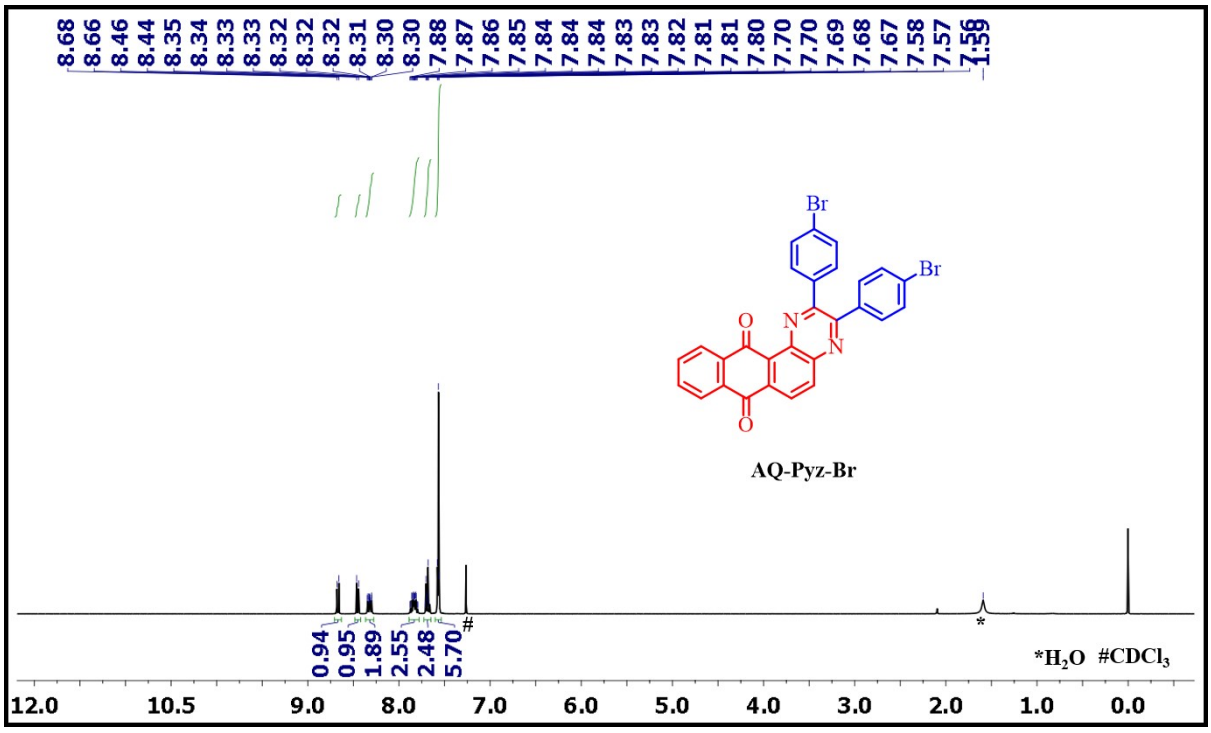

Fig. S1. ^{1}H NMR spectra of AQ-Pyz-Br.

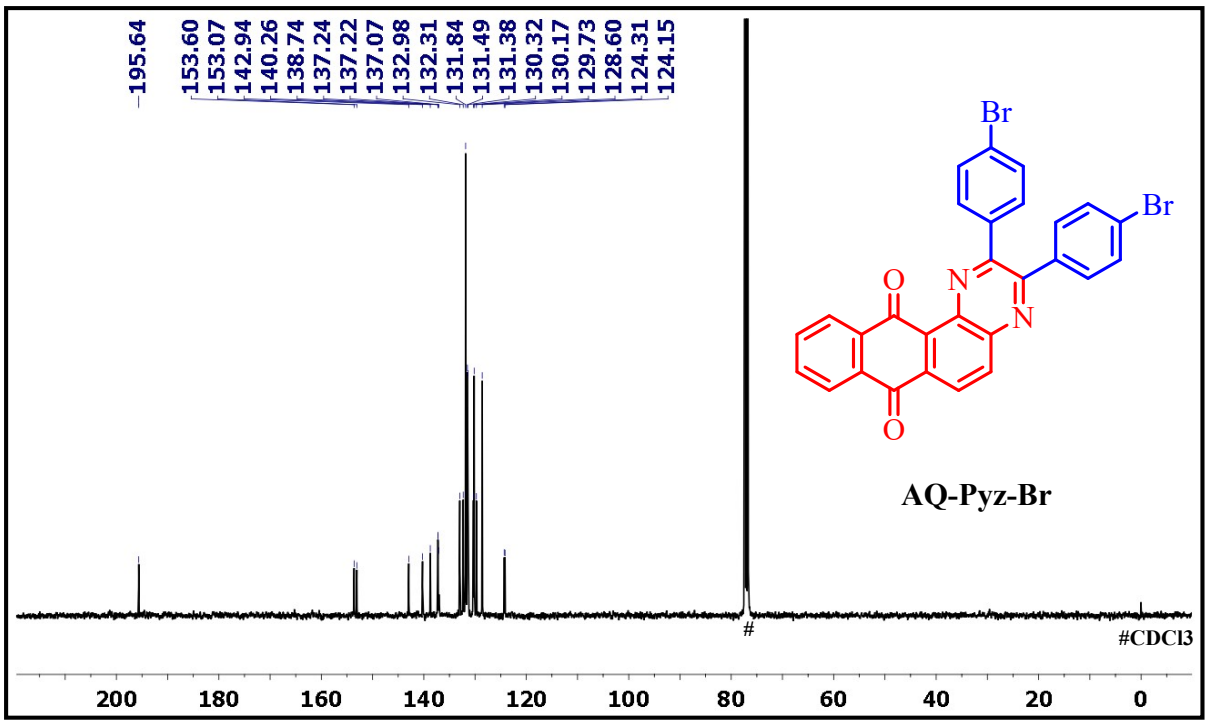

Fig. S2. ^{13}C NMR spectra of AQ-Pyz-Br.

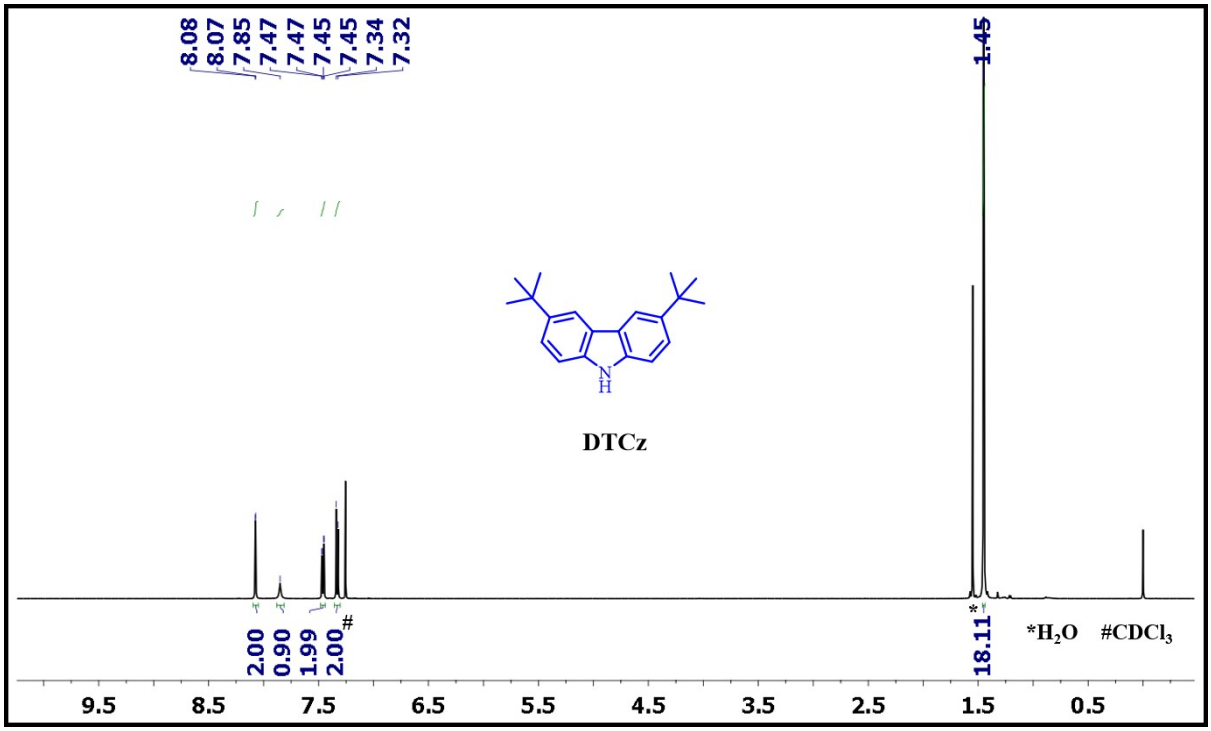

Fig. S3. ^{1}H NMR spectra of DTCz.

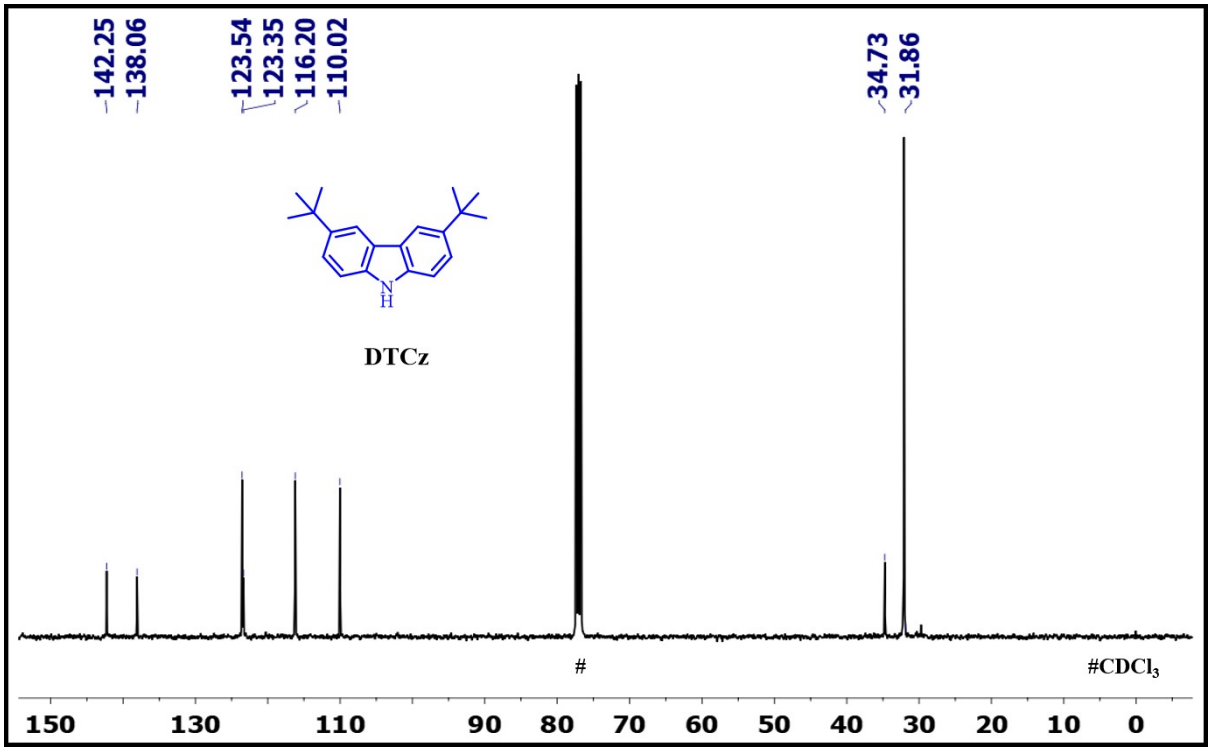

Fig. S4. ^{13}C NMR spectra of DTCz.

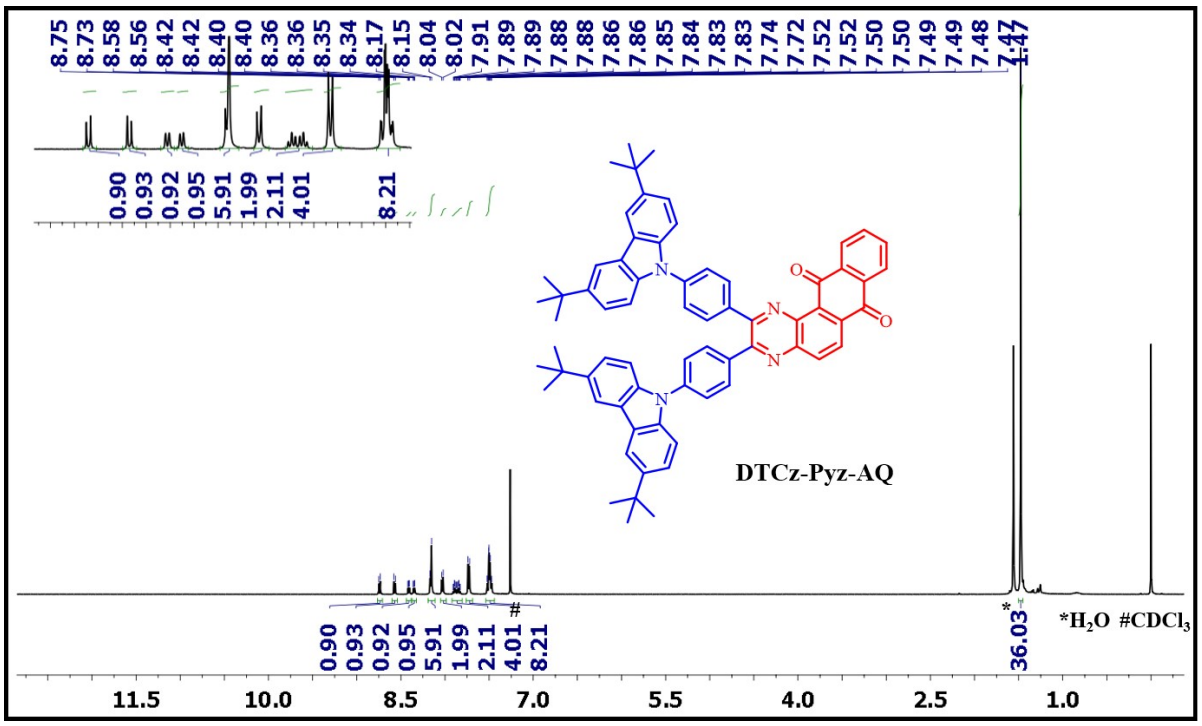

Fig. S5. ^{1}H NMR spectra of DTCz-Pyz-AQ

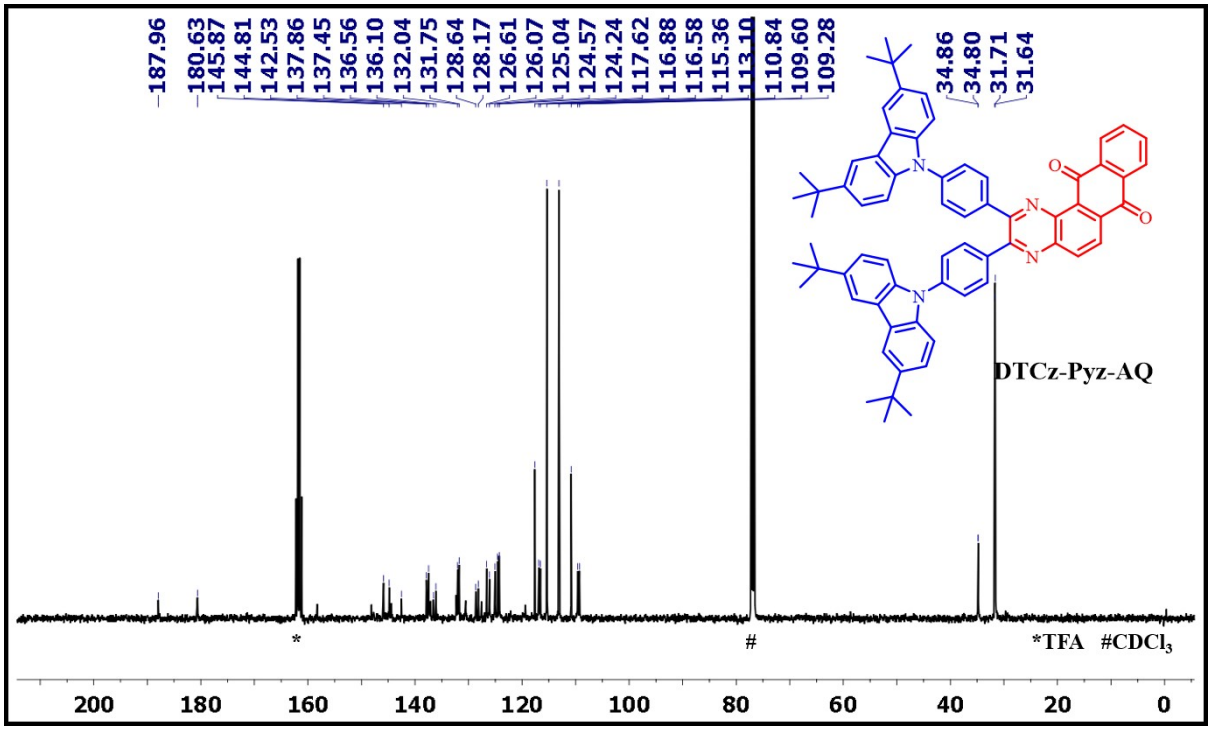

Fig. S6. ^{13}C NMR spectra ofDTCz-Pyz-AQ.

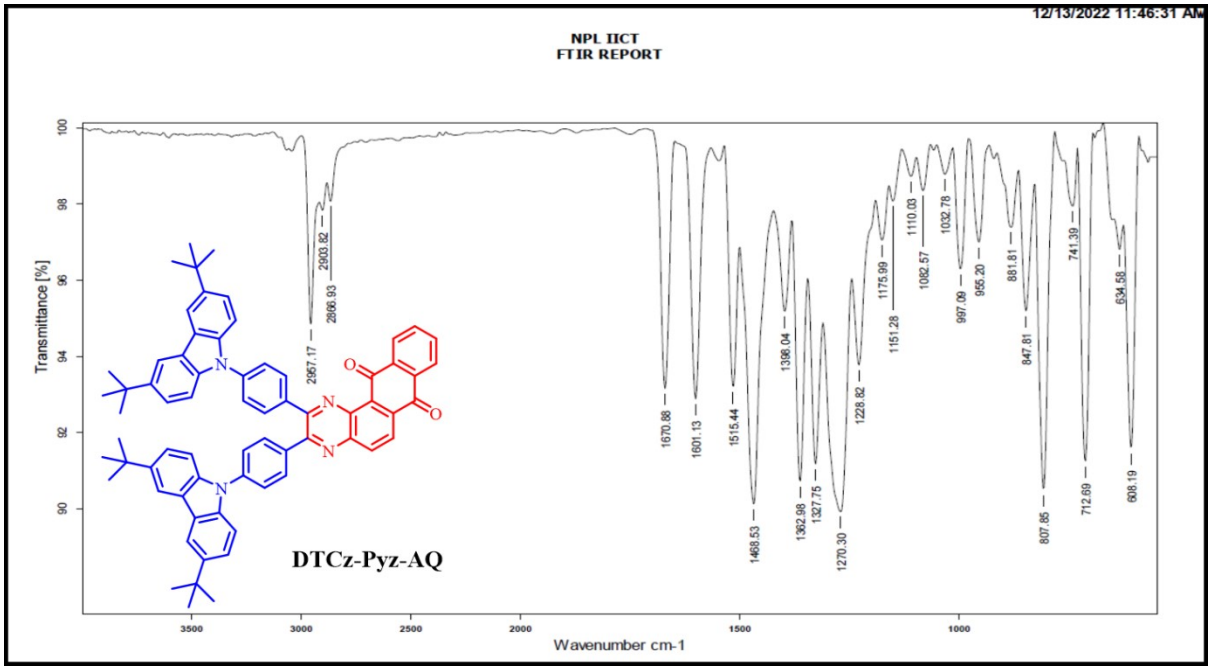

Fig. S7. FT-IR spectra of DTCz-Pyz-AQ.

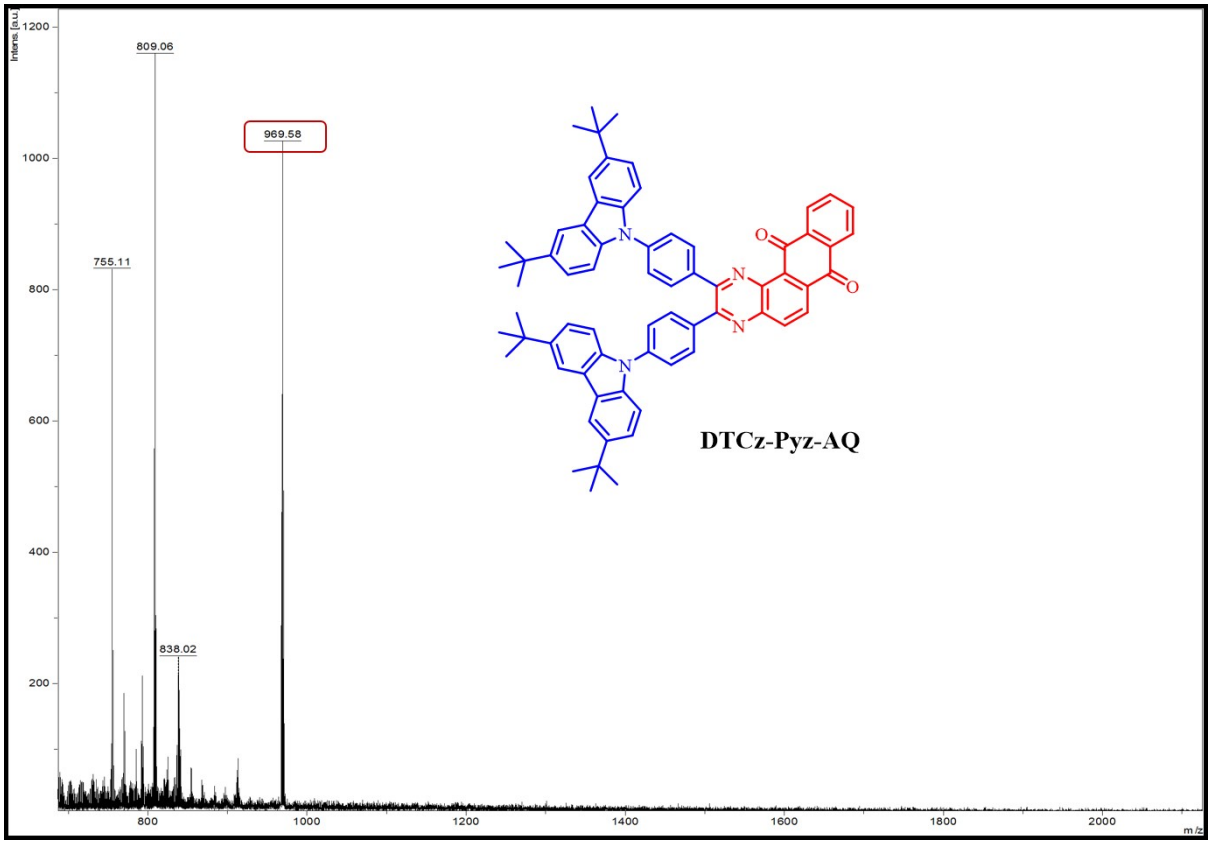

Fig. S8. MALDI-TOF spectrum of DTCz-Pyz-AQ.

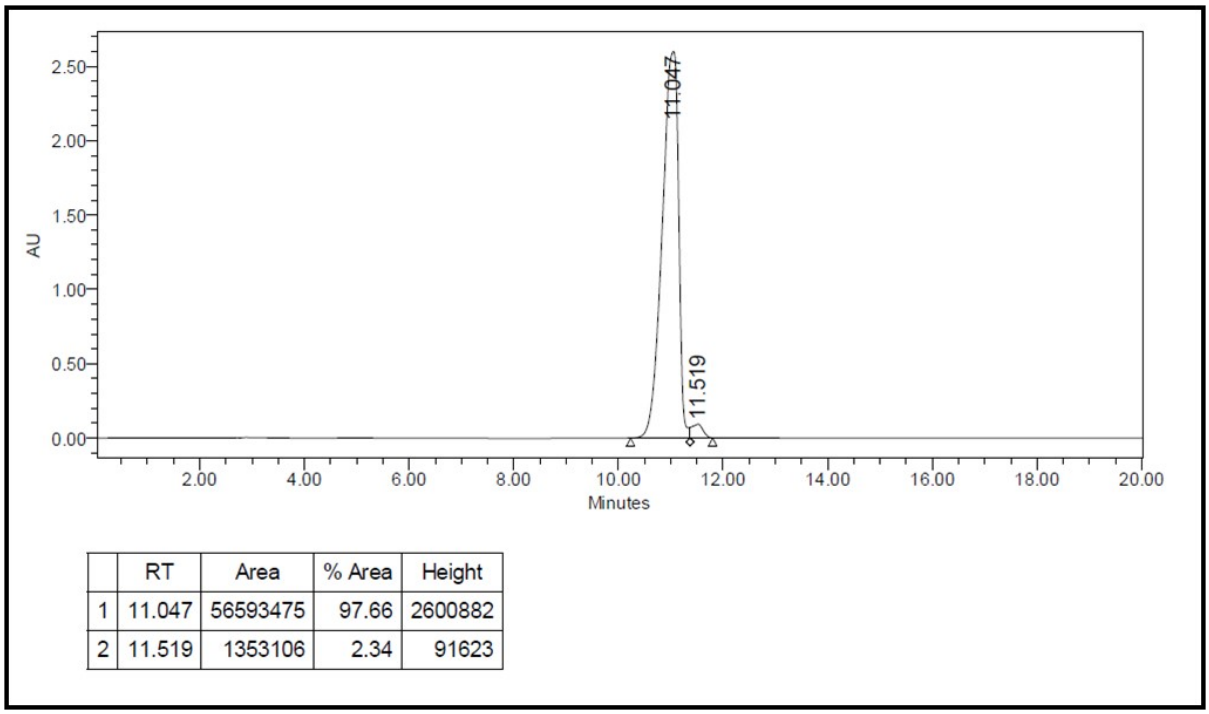

	RT	Area	% Area	Height
1	11.047	56593475	97.66	2600882
2	11.519	1353106	2.34	91623

Fig. S9. HPLC chromatography of DTCz-Pyz-AQ.

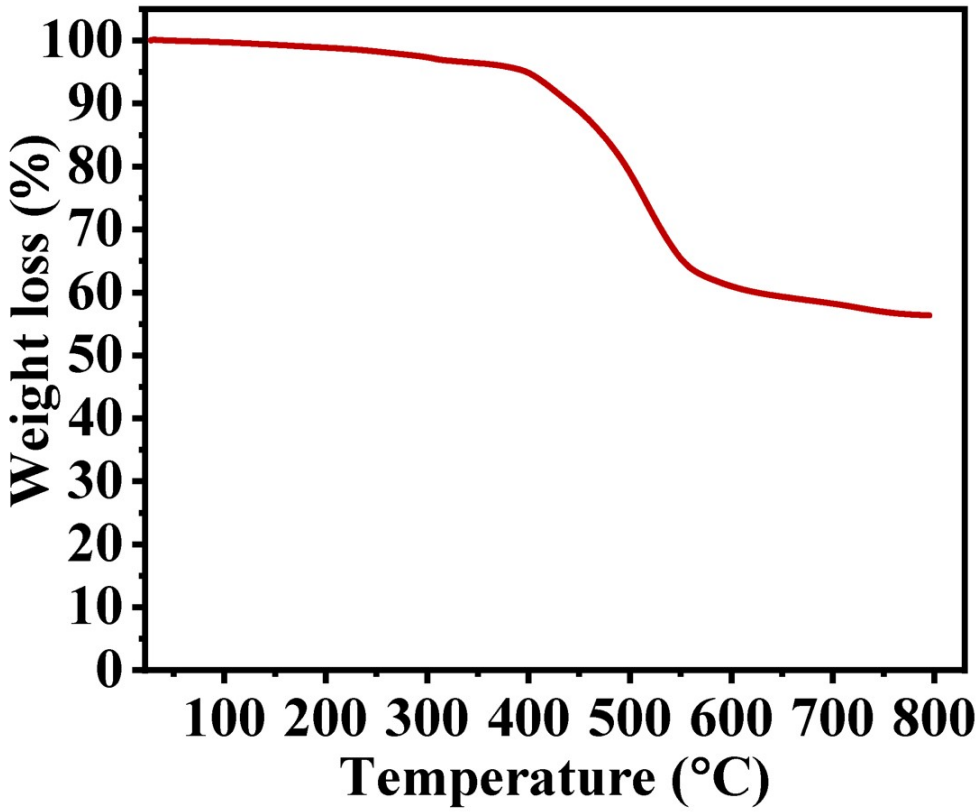

Fig. S10. Thermogravimetric analysis (TGA) of DTCz-Pyz-AQ.

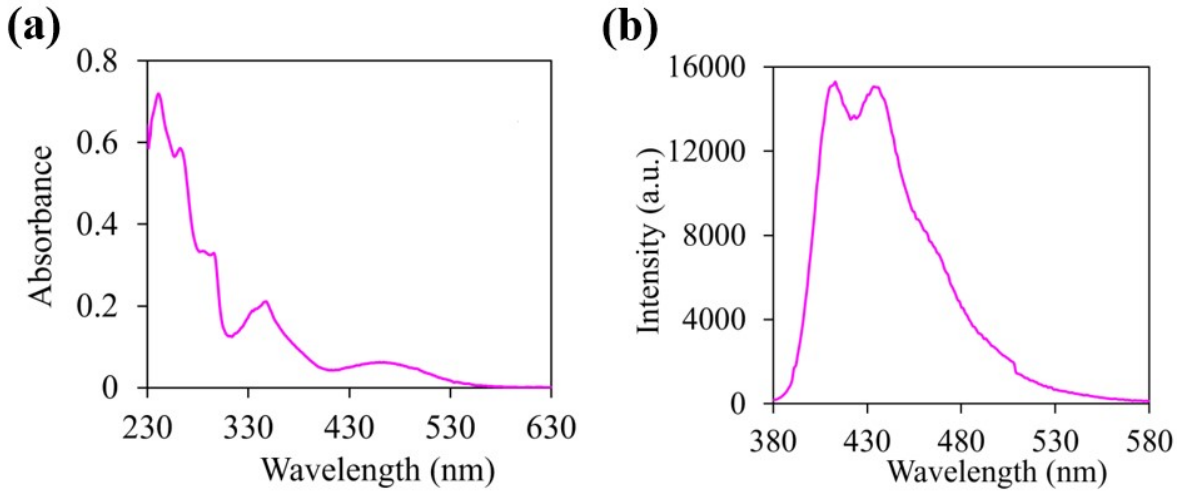

Fig. S11. a) UV-Vis absorption spectra; b) Emission of the DTCz-Pyz-AQ λ_{ex} at 370 nm in DCM solution (1×10^{-5} M).

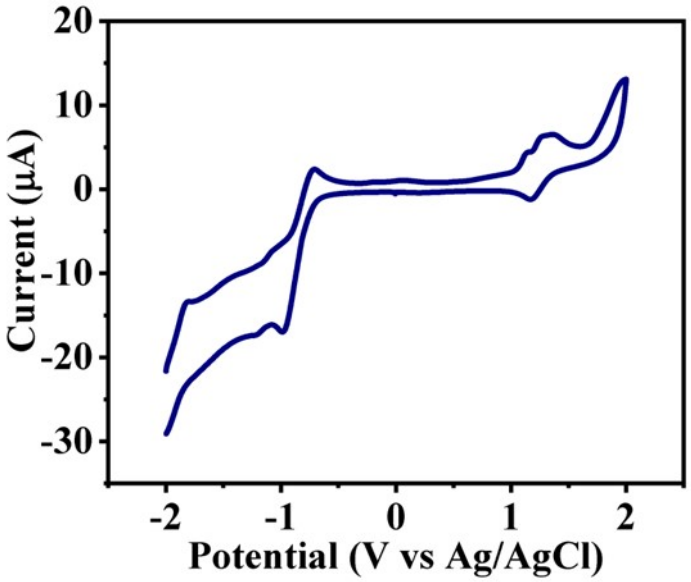

Fig. S12. Cyclic voltammogram (CV) of DTCz-Pyz-AQ in dichloromethane with 0.1 M tetrabutylammonium hexafluorophosphate electrolyte. The data was recorded at 10 mV s^{-1} scan rate:

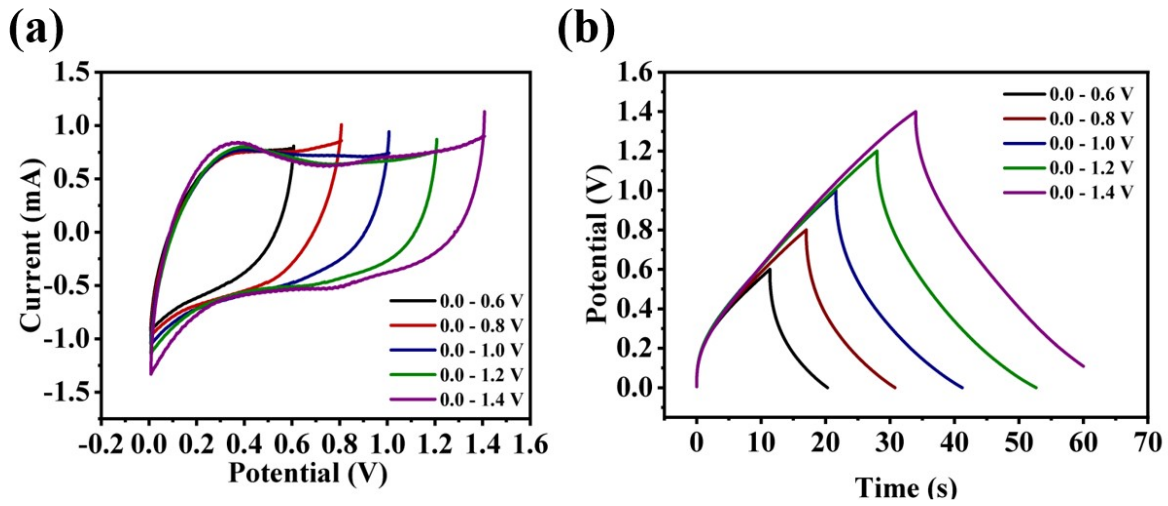

Fig. S13. (a) CVs of the DTCz-Pyz-AQ/GF//DTCz-Pyz-AQ /GF device measured at various potential at a scan rate of 10 mV s^{-1}; (b) GCD curves at fixed current density 1A g^{-1} for the DTCz-Pyz-AQ//DTCz-Pyz-AQ device measured at different potential windows.

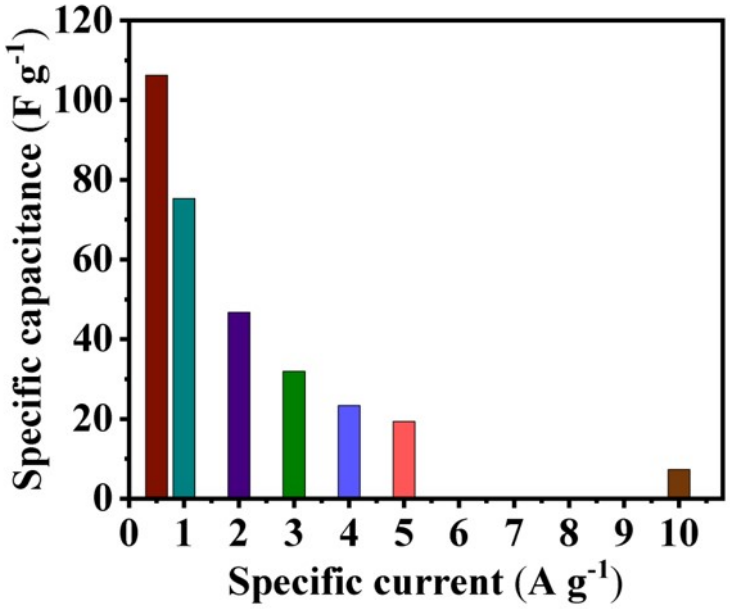

Fig. S14. Specific capacitance at specific current density 0.5, 1, 2, 3, 4, 5, and 10 A g^{-1} for symmetric cell device DTCz-Pyz-AQ/GF//DTCz-Pyz-AQ /GF

Table S1. Specific capacitance (C_{sp}) of DTCz-Pyz-AQ/GF based SC device from CV and GCD profiles at different scan rate and current density (three-electrode system).

Scan rate mVs^{-1}	**Specific capacitance (Fg^{-1})**	**Current density (Ag^{-1})**	**Specific capacitance (Fg^{-1})**
5	227.48	0.5	304.37
10	185.12	1	242.50
20	144.30	2	162.25
30	123..05	3	121.55
50	90.93	4	99.99
100	51.50	5	86.68
200	26.79	10	52.53

Table S2. Specific capacitance (C_{sp}) of DTCz-Pyz-AQ/GF//DTCz-Pyz-AQ/GF symmetric supercapacitor device from GCD profiles at different current densities, specific energy, and specific power.

GCD analysis		**Specific energy density**	**Specific power density**
Current density (Ag^{-1})	**Specific capacitance** (Fg^{-1})	$(Whkg^{-1})$	(Wkg^{-1})
0.5	106.30	15.94	899.71
1	75.31	11.29	1799.20
2	46.74	7.01	3600.00
3	31.89	4.78	5400.00
4	23.32	3.49	7200.00
5	19.36	2.90	8996.90
10	7.30	1.09	18000.00

Table S3. EIS fitted parameter for DTCz-Pyz-AQ/GF//DTCz-Pyz-AQ/GF in two-electrode system.

Parameters	$R_s(\Omega\ cm^2)$	$R_{ct}(\Omega\ cm^2)$	$C_{pe}(F\ cm^2)$
DTCz-Pyz-AQ/GF//DTCz-Pyz-AQ/GF	2.52	709	0.436

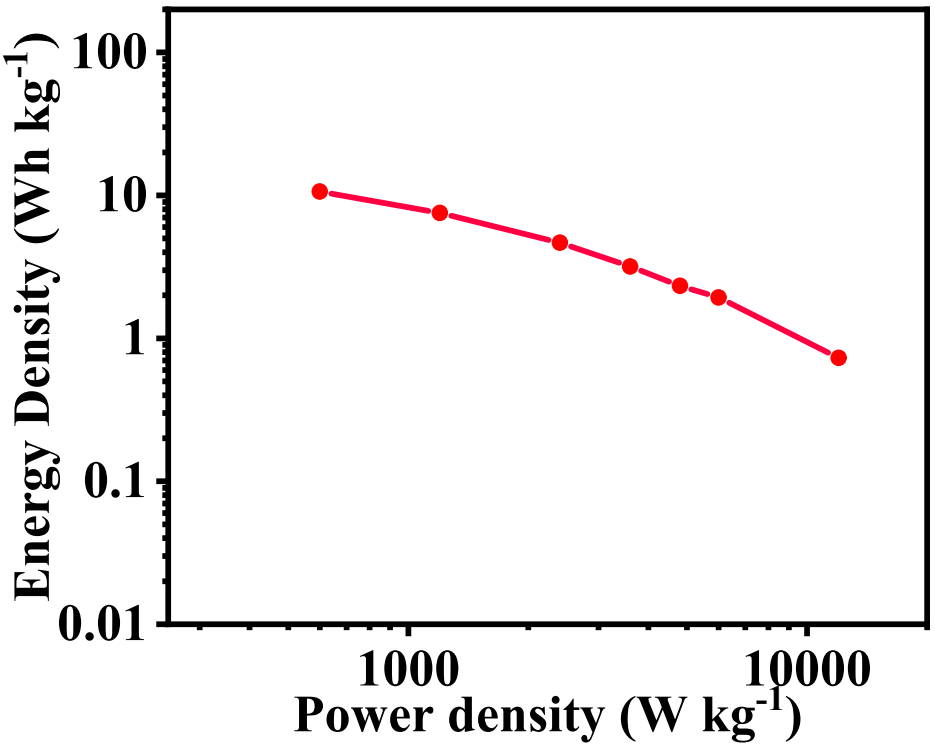

Fig. S15. Ragone plot for the DTCz-Pyz-AQ/GF//DTCz-Pyz-AQ/GF SSC device.

The SSC cell still maintain an energy density of 1.09 Wh kg^{-1}, even at a high power density value of 18000 W kg^{-1}. On the basis of the above electrochemical results, we found that the electrode materials based on DTCz-Pyz-AQ/GF exhibited high C_{sp} and stable cycle life, suggesting D-A-A molecular architecture should be considered as a novel type of pseudocapacitive material for high energy storage applications.

SEM images of the Electrode Materials

Furthermore, scanning electron microscopy (SEM) technique was used to establish the physical stability of the electrode before and after 6000 GCD cycles. The surface morphology of DTCz-Pyz-AQ/GF electrode material can be observed from the SEM images before and after 6000 GCD cycles. As given in Fig. S14a(i) and S14a (ii), the SEM image shows the irregular fiber like morphology of the electrode. After 6000

GCD cycles, the fiber like morphology remains unaltered Fig.S14 b(i) and S14 b (ii). Therefore, we presume that the physical stability of the electrodes based on DTCz-Pyz-AQ/GF is responsible for the excellent device performance.

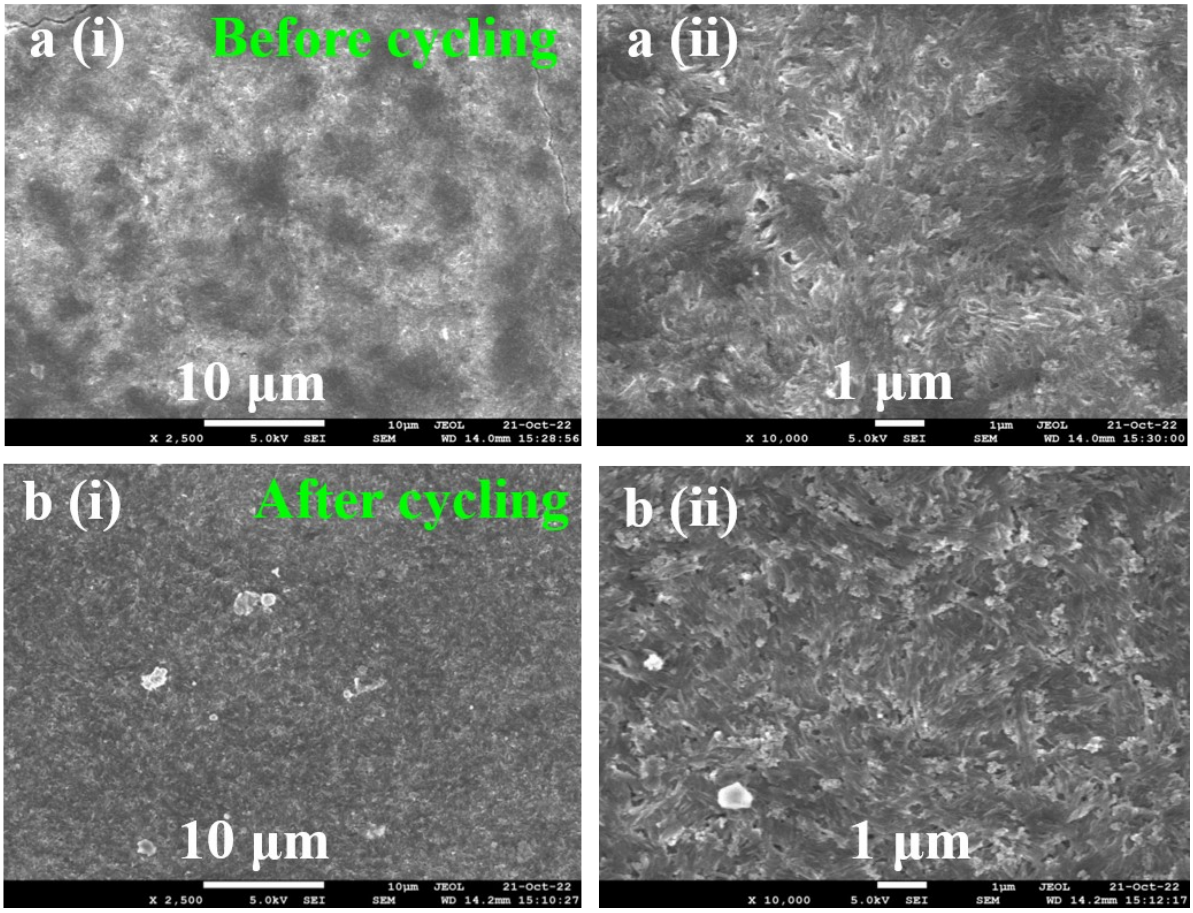

Fig. S16. SEM images of the DTCz-Pyz-AQ/GF electrode materials [a (i) and a (ii)] before GCD cycles and [b (i) and b (ii)] after cycling performance in DTCz-Pyz-AQ/GF//DTCz-Pyz-AQ/GF based SSC device.

FT-IR spectra of electrode before and after 6000 GCD cycles

Chemical stability of the electrode was established by employing FT-IR spectroscopic technique. FT-IR peaks of the electrode before (Fig.17a) and after 6000 GCD cycles (Fig.17b) showed there is no change in peak positions, indicating the DTCz-Pyz-AQ material is chemically stable.

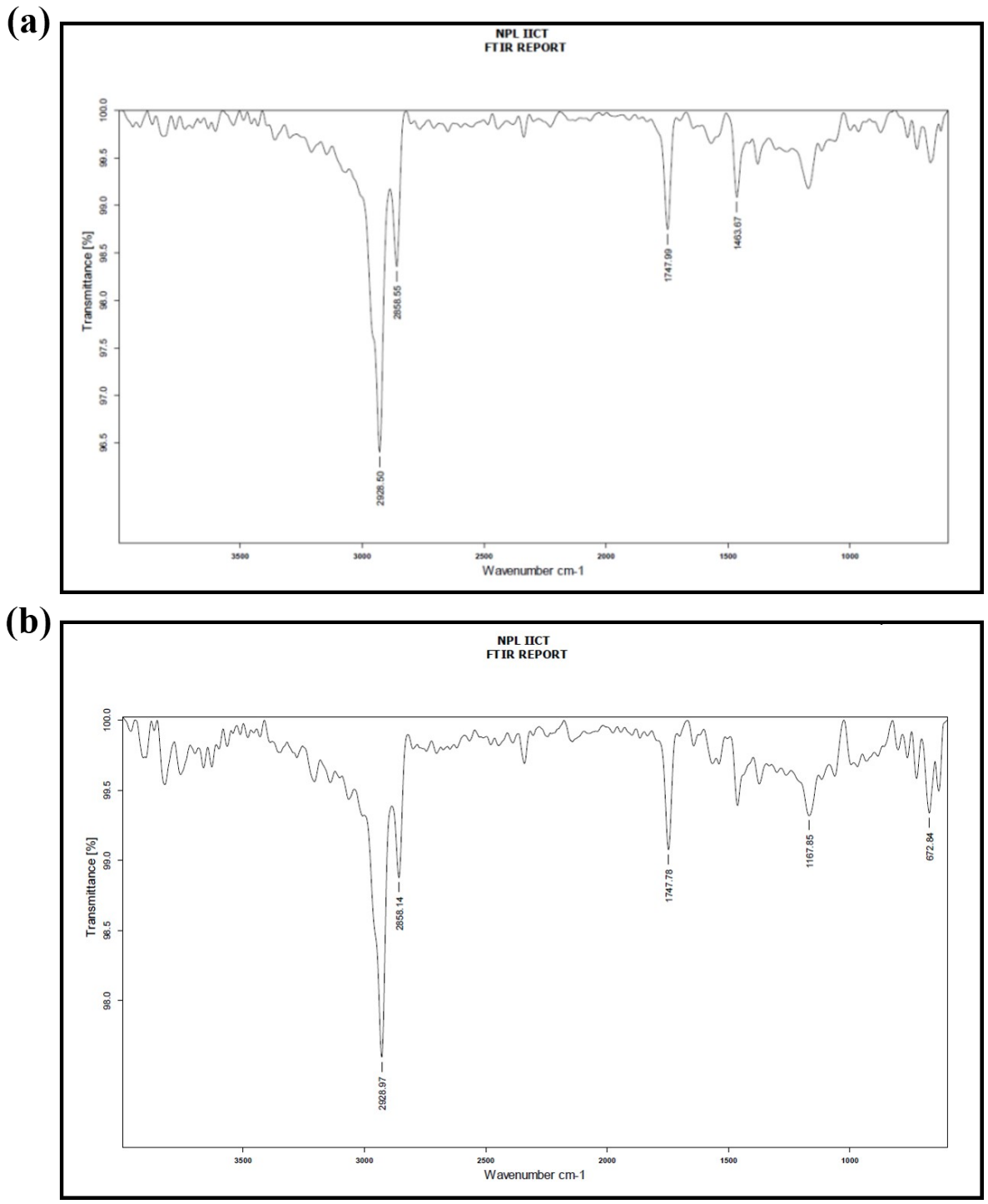

Fig. S17. FT-IR spectrum of DTCz-Pyz-AQ (a) before and (b) after 6000 GCD cycles.

Table S4. Comparative SC data from literature and DTCz-Pyz-AQ/GF//DTCz-Pyz-AQ/GF.

Sr. No	Electrode Material	Electrolyte	Voltage (V)	Current density ($A\ g^{-1}$)	Csp GCD ($F\ g^{-1}$)	Energy density ($Wh\ Kg^{-1}$)	Power density ($W\ kg^{-1}$)	N^{th} cycles @ current density ($A\ g^{-1}$)	C_{sp} Retention (%)	Ref No.
1.	Pyz-ANQ/CP//Pyz-ANQ/CP	1 M H_2SO_4	0 to 0.8	0.5	36.6	5.1	4700	2,000 @ 4	78.4[a]	S3
2.	rGO-n-IDT	PVA/ H_2SO_4	-0.2 to 1.0	1	489.6	3.7	101	10,000 @ 10	91[a]	S4
3.	HTCP-700/CP//HTCP-700/CP	1 M H_2SO_4	0 to 1.2	1	445	11.6	6000	5,000 @ 1	86[a]	S5
4.	AQS@rGO//rGO	1 M H_2SO_4	-0.3 to 0.4 V	1	477.6	29.2	3420	10,000 @ 5	83.10[b]	S6
5.	Cz-TPA CMP	1 M H_2SO_4	0.1 to 0.6	0.5	271.82	-	-	2,000 @ 10	98.87 [b]	S7
6.	CBz-PANI/Au@PET//CBz-PANI/Au@PET	1 M H_2SO_4	0.0 to 0.7	0.8	319.00	2.45	2.71	10,000 @ 0.5	83[a]	S8
7.	NQ-DP/GF// NQ-DP/GF	1 M H_2SO_4	0 to 1.2	0.5	177.9	6.0	600	6,000 @ 1	97.9[a]	S9
8.	AQ-NPCs//TN-NPCs	1 M H_2SO_4	0.0 to 1.4 V	1	86.0	23.5	700	5,000 @ 5	75.30[b]	S10
9.	DTCz-Pyz-AQ /GF// DTCz-Pyz-AQ /GF	**1 M H_2SO_4**	**0 to 1.2**	**0.5**	**106.30**	**15.94**	**899.71**	**6,000 @ 2**	**93.80[a]**	**Present Work**

Where [a]- symmetric two electrode system, and [b]- asymmetric two electrode system.

References

S1.R. Velayuthama, R. Manikandana, C.J. Raj , A. M. Kale, C. Kayac, K. Palanisamye, B. C. Kim, *J. Alloys Compd*, **863** (2021) 158332.

S2.J. Yu, N. Fu, J. Zhao, R. Liu, F. Li, Y. Du, and Z. Yang, *ACS Omega*, 2019, **4,** 15904−15911.

S3.M. R. Biradar, A. V. Salkar, P. P. Morajkar, S. V. Bhosale, and S. V. Bhosale, *J. Energy Storage*, 2022, **48,** 103953.

S4.B. Pan, L. Bai, C. Hu, X. Wang, W. Li, and F. Gang Z, *Adv. Energy Mater,* 2020, **10,** 2000181.

S5.N. Deka, J. Deka and G. K. Dutta, *ChemistrySelect*, 2018, **3**,8483–8490.

S6.R. Shi, C. Han, H. Duan, L. Xu, D. Zhou, H. Li, J. Li, F. Kang, B. Li, and G. Wang, *Adv. Energy Mater.*, 2018, **8,** 1802088.

S7.B. Luo, Y. Chen, Y. Zhang and J. Huo, *New J. Chem.,* 2021, **45,** 17278

S8.M. Almtiri, T. J. Dowell, H. Giri, D. O. Wipf, and C. N. Scott**,** *ACS Appl. Polym. Mater*. 2022, **4,** 3088−3097.

S9.M. R. Biradar, A. V. Salkar, P. P. Morajkar, S. V. Bhosale and S. V. Bhosale, New J. Chem., 2021, **45,** 5154–5164.

S10.B. Guo, Y.Yang, Z. Hu, Y. An, Q. Zhang, X Yang, X. Wang, H. Wu, *Electrochimica Acta*, **223,** (2017) 74–84.